Hindawi
International Journal of Polymer Science
Volume 2019, Article ID 8402518, 15 pages
https://doi.org/10.1155/2019/8402518

Research Article

Predictable Behavior of GFRP-Reinforced Bridge Decks: Formulation of a Strain-Based Capacity Model

Young Hoon Kim,[1] **Yeesock Kim**,[2] **and Yeonho Park**[3]

[1]*Civil and Environmental Engineering, The University of Louisville, Louisville, Kentucky, USA*
[2]*Civil Engineering and Construction Management, California Baptist University, Riverside, California, USA*
[3]*Civil Engineering, The University of Texas at Arlington, Texas, USA*

Correspondence should be addressed to Young Hoon Kim; yhkim005@louisville.edu

Received 30 August 2018; Revised 6 February 2019; Accepted 3 April 2019; Published 15 May 2019

Academic Editor: Ulrich Maschke

This paper proposes a reliability analysis framework for glass fiber-reinforced polymer- (GFRP-) reinforced concrete systems with uncertain capacities and demands over time. Unfortunately, there has been limited discussion or research done related to the potential change of failure modes over time. Therefore, a rational approach is needed to integrate multiple failure modes in a single analysis framework, considering uncertainties of time-variant demands and capacities. To account for multiple failure modes, this study proposes the limit state function to estimate the safety margin, based on strain values of GFRP-reinforcing bars. A proposed limit state function can capture the likelihood of both shear and flexural failure modes, simultaneously. In this study, seven typical bridge deck configurations (e.g., varied deck thickness, girder spacing, and bar size) were exposed to various ambient temperatures. Simulation results show that reliability indices of 100-year exposure exhibit significant variance, ranging from 2.35 to 0.93, with exposure temperatures ranging from 13 to 33°C. Exposure temperature and time are the dominant factors influencing the reliability indices, so are the ones that need to be changed. As exposure time and/or exposure temperature increase, the flexural capacity model plays an important role to determine the reliability indices. When flexural and shear failure modes are equally dominant, reliability indices can capture risks of both failures, using the proposed strain-based approach.

1. Introduction

1.1. General. Engineers and researchers have made significant progress toward standardizing test methods and designs for structural elements, using composite reinforcement [1, 2]. In 2009, the American Association of State Highway Officials (AASTHO) approved the use of glass fiber–reinforced polymer (GFRP) in bridge decks. The Canadian Highway Bridge Design Code (CSA S6-06 [3]) allows the use of carbon fiber–reinforced polymer (CFRP) for primary reinforcement and prestressing tendons in concrete. Research communities concur that fiber-reinforced polymers (FRPs) are materials that have multiple benefits, including, but not limited to, high specific strength, enhanced fatigue life, resistance to corrosion, controlled thermal properties, nonmagnetic properties, and potentially lower life cycle costs [4–6]. Their application has gained momentum for use in bridge decks, pavements, walls, and beam-column joint systems [4–6]. Therefore, it follows that the potential applications of composite reinforcement for structural elements will increase. However, current designs are not calibrated with the realistic performance of FRP embedded in concrete, and the temperature effect is not included in current practice. Based on two categories of exposure conditions, the constant (time-invariant) reduction factor was selected to account for the potential reduction of tensile capacity over time [4–6]. Contrary to the steel-reinforced systems subjected to corrosive environments, there has been minimal research regarding FRP-reinforced systems; therefore, there is little knowledge or understanding of the time-variant mechanism of FRP-reinforced systems. The service life of FRP-reinforced concrete systems should be realistically predicted as the first step

toward designing a performance-based, sustainable structure. This paper's goal is to facilitate the prediction of the service life of the system with various design parameters, using uncertainties of capacity and demand.

1.2. Bridge Deck Design. In conventional design practices, the design of a bridge deck primarily focuses on required flexural design in accordance with AASHTO specifications [1, 2]. Shear reinforcement is not required for either steel-reinforced or FRP-reinforced bridge decks. Steel-reinforced bridge decks are typically designed as tension-controlled sections and are analyzed using a unit-wide strip deck model with a rectangular cross section. In addition, it is generally accepted that the shear failure mode is a punching-shear mode rather than a one-way shear mode. Therefore, one-way shear failure is usually not considered in steel-reinforced bridge deck design. Arch action can prevent one-way shear failure and flexural failure by distributing the wheel loads to adjacent supporting girders. Therefore, two-way shear failure may occur with six to seven times the design service wheel loads. However, Rodrigues et al. [7] reported that shear failure can be dominant in the slender members with flexural reinforcement. Shear failure cannot develop in members whose flexural reinforcement remains elastic (statically determinate beam), but can develop once the flexural strength is reached, resulting in reinforcement yielding (i.e., continuous beam or slab). This is also identified in the statically indeterminate structure (i.e., continuous beam or slab) [8]. A recent study also quantified shear strength in a reinforced concrete system using strain measurements [9–11] and RC beams under shear strengthened carbon fiber-reinforced polymer U-stirrup system [12]. Hu and Wu [9] concluded that shear strength of concrete, V_c, is significantly varied with and without shear reinforcement. Especially, the difference can be significant when the span-to-depth ratio is over 2.5, i.e., a/d value > 2.5 (such as a slender member) in the predicted and measured values [9]. Therefore, one-way shear failure cannot be neglected in the design of a conventional bridge deck, which is a continuous slab. It draws more attention to one-way shear failure of steel-reinforced bridge decks. Recently, shear behavior of steel-reinforced concrete members is estimated using strain-based methods for the slender beam which tends to fail in concrete crushing within the compression zone [13–15]. The proposed model [16] can consider both tensile reinforcement ratio and concrete compressive strength. This suggests that the strain-based approach can be useful for considering multiple failure modes in reliability analysis. Similarly, the author's approach will be discussed in the following section.

Additional research is needed on FRP-reinforced bridge decks. Several researchers have performed studies on bridge decks, using FRP reinforcement. El-Sayed et al. [17] reported that a tested bridge deck is more likely to fail because of one-way shear than flexural failure. In an independent research, Ashour [18] reported that an overreinforced beam failed in the shear, even though the specimen was initially designed as a flexural member. In addition, Amico [19] reported the shear failure of a one-way slab used as a weigh station, with GFRP reinforcement used as the top-mat reinforcement. The observed failures were shear dominant and/or concrete-crushing failures. There are marginally small gaps between a flexural failure and a one-way shear failure. From several experimental results, it has been determined that a one-way shear failure should be considered in the structural risk and reliability assessment. Even though two-way shear failure can be considered as the critical failure mode [20], one-way shear failure should be assessed from the aspect of reliability. Hassan and Rizjalla [20] pointed out that two-way shear failure is more than likely failure mode in simulation and experimental testing.

In the flexural design of steel-reinforced bridge decks (i.e., generally $t = 0$), the target reliability index is 3.5 to 4.0 for compression-controlled sections. With the given section, the strength reduction factor, ϕ, is calibrated to be 0.65 for steel-reinforced concrete members [21]. In the GFRP-reinforced member, both ϕ and the environmental reduction factor, C_E, may need to be calibrated. The value of C_E (i.e., multiplier 0.7 or 0.8 of guaranteed tensile strength, $f_{fu}^* = f_{fu,\text{ave}} - 3\sigma$, where $f_{fu,\text{ave}}$ is the mean tensile strength of sample of test specimens and σ is the standard deviation) is used to account for the reduction of bar capacity, resulting from high-alkali pore solutions in concrete and the aging effect. In current practice, the value of C_E has been adopted based on the results of tensile strength tests exposed to accelerating and aggressive environmental conditions. When calibrating a strength reduction factor, the current practice is to adopt $C_E = 0.8$. Using C_E of 0.8 for the GFRP bars, the ACI 440 committee decided to reach the target reliability index of 3.5 for flexure, regardless of failure mode. To achieve this, the tension-controlled section design needs to use ϕ of 0.55 to maintain the reliability index of 3.5. The reliability indices range between 3.45 and 4.01 for the below 1.55 times balanced reinforcement ratio, ρ_{fb}. [22]. Shield et al. [22] reported that the probability of FRP bar failure is greater than for concrete crushing failure. The difference decreases as the reinforcement ratio approaches $1.55\rho_{fb}$. However, this approach does not account for different degradation scenarios coupled with shear failure mode. The constant-value-based approach (i.e., time-invariant) was used to calibrate the strength reduction factor to achieve the reliability index. Therefore, further research is needed to calibrate these factors in a framework of performance-based approach as a function of exposure time and exposure conditions.

1.3. Improved Models and Analysis. In a recent article, the first author of this paper presented focused on the strength-based reliability analysis (Kim et al. [23]), as presented inside solid boxes in Figure 1. However, the analysis formulation is limited in only flexural capacity and the deterministic demand model-based fragility curves. In this study, substantial changes were made by incorporating shear failure and the time-variant demand model into the previous analysis framework (dashed boxes in Figure 1). Since one-way shear failure cannot be underestimated, based on Rodrigues et al.'s [7] findings, the probability of one-way shear failure is considered in this study. It should be noted that two-way shear failure is not included in this study. According to the performance-based durability design concept of Flint et al.

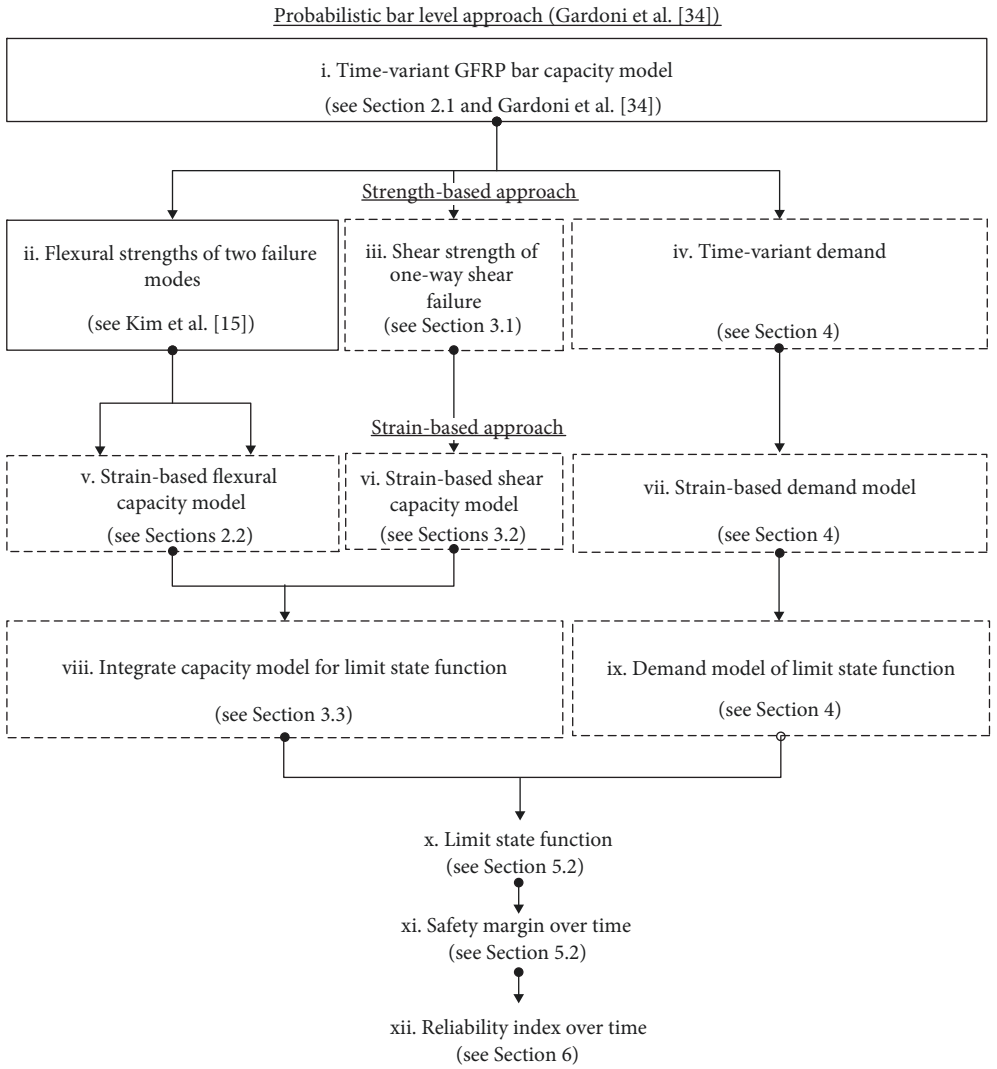

Figure 1: Flowchart of framework.

[24], the performance-based model is formulated from the integration of mathematical models of the interests rather than the application of prescriptive approaches (e.g., limiting acceptable performance). Therefore, efforts of this research aim to contribute to this area.

This paper consists of seven parts. Section 1 presents an overview of current designs and justifications of one-way shear capacity in steel and FRP-reinforced bridge decks. Section 2 briefly presents the formulation of strain-based models for flexural capacity (see item v of Figure 1). Section 3 presents the probabilistic one-way shear capacity model in both strength and strain-based models (see items iii and vi in Figure 1). Section 4 presents the time-variant demand model (see items iv and vii in Figure 1). Section 5 presents the parametric study of various design cases. This demonstrates the change of strain-based safety margins with time-variant properties of GFRP bars (see items viii and ix in Figure 1). Section 6 presents the reliability indices of GFRP-reinforced bridge decks of various designs and three representative exposure temperatures (see item xii in Figure 1). Finally, Section 7 presents the conclusions and recommendations.

2. Formulation of the Strain-Based Model (Flexural)

2.1. Time-Variant GFRP Bar Capacity Model. Even though GFRP reinforcements do not exhibit the classical corrosion observed in steel, several researchers [25–27] have reported a significant reduction in the tensile capacity of GFRP reinforcement when it is exposed to aggressive solutions and exposure conditions (e.g., high pH, salt water, high temperatures, freeze-thaw cycles, and wet/dry cycles). A field study conducted by Mufti et al. [28, 29] and Benmokrane and Cousin [30] concluded that GFRP reinforcement is durable when embedded in concrete. Concrete cores with GFRP reinforcement, which had been embedded in concrete for five to eight years, were removed from five locations in Canada (Quebec, Ontario, Alberta, British Columbia, and Nova Scotia). Recent findings [31] indicate that the interface of fiber and matrix are prone to initiating damage in high temperatures. Similar debonding was also reported by Benmokrane et al. in 2006 [32]. Still, researchers have debated the durability of GFRP systems,

and data is limited on a realistic estimation of the reduction of capacity and its reliability.

Recently, Park et al. [33] reported that different types of GFRP reinforcement exhibited different rates of degradation of flexural capacity when embedded in concrete under the same exposure conditions. Therefore, a probabilistic model is needed to capture the diverse degradation rates and to propose the robust model.

To perform the time-variant reliability analysis, Gardoni et al. [34] developed the following probabilistic time-variant model to predict the capacity of GFRP bars embedded in concrete as follows:

$$\sigma_t(\mathbf{x}_b, \boldsymbol{\Theta}_\sigma) = \left\{ (1 + s_0 e_0) - \lambda \left[\frac{\left(D_{T_{23}} \exp\left[(E_a/R)(1/T_{23} - 1/T)\right]t\right)}{r^2} \right]^{\alpha} (1 + se) \right\} \mu_{\sigma_0}, \tag{1}$$

where $\mathbf{x}_b = (D_{T_{23}}, E_a, R, r)$ is a vector of basic variables (i.e., material properties, geometry, and temperature), $D_{T_{23}}$ = the diffusion coefficient at a defined reference temperature, T_{23} = 296 K (23°C), E_a = the activation energy (KJ), R = the universal gas constant (KJ/mol-K), r = the radius of the GFRP reinforcement, T = the exposure temperatures (in K), $s_0 e_0$ is the error term that captures the variability of s_0 around its mean μ_{σ_0} ($= f_{fu,\text{ave}}$), and se is the error term that captures the variability in the reduction term, $[(D_{T_{23}} \exp[(E_a/R)(1/T_{23} - 1/T)]t)/r^2]^{\alpha}$. The terms e_0 and e are statistically independent, identically distributed random variables with a mean and unit variance of zero, s_0 and s are the standard deviations of the two error terms, and $\boldsymbol{\Theta}_\sigma = (\lambda, \alpha, R, s_0, s)$ is a vector of unknown parameters introduced to fit the data. Two assumptions are made in formulating the model: (a) s_0 and s are not functions of $\mathbf{x}_b$ (homoscedasticity assumption), and (b) e_0 and e each have normal distributions (normality assumption).

A Bayesian approach was used to estimate the statistics (means and covariance matrices) of the unknown parameters $\boldsymbol{\Theta}_\sigma$ based on long-term exposure data (up to 7 years of exposure to actual environmental conditions) for GFRP bars from three different manufacturers. The posterior statistics of $\boldsymbol{\Theta}_\sigma$ are reported in Gardoni et al. [34].

Using the time-variant bar capacity model, Kim et al. [23] conducted research to investigate the impact of reducing tensile capacity on the flexural capacity and the probability of failure over time. The following equation is used to estimate the flexural capacity, $C_t(\mathbf{x}, \boldsymbol{\Theta}) = \min[C_{\text{CF},t}(\mathbf{x}, \boldsymbol{\Theta}), C_{\text{BF},t}(\mathbf{x}, \boldsymbol{\Theta})]$, where $C_{\text{CF},t}(\mathbf{x}, \boldsymbol{\Theta})$ and $C_{\text{BF},t}(\mathbf{x}, \boldsymbol{\Theta})$ are the nominal moment capacity of concrete crushing failure and bar failure, where $\boldsymbol{\Theta}$ and $\mathbf{x}$ are the vectors to capture the parameters to estimate nominal moment capacities and parameters, $\boldsymbol{\Theta} = (\boldsymbol{\Theta}_\sigma, \boldsymbol{\Theta}_E)$, respectively, where $\boldsymbol{\Theta}_E$ is a vector of unknown parameters to fit the data of elasticity of concrete [35].

2.2. Strain of GFRP Bars at Flexural Failure. Figure 2 shows the strain distribution of the section of FRP-reinforced concrete deck in three different failure modes.

Capacities of bars in the unit-wide strip deck were assumed to be statistically independent and identically distributed random variables. The capacity of each bar was totaled to determine the moment capacity of the section.

The strain of GFRP reinforcement was determined by the two failure modes: concrete crushing failure and bar failure. When bar failure is dominant, the maximum strain in the concrete (which is defined here as ε_c) at the bar failure is smaller than the ultimate strain, ε_{cu}. To determine ε_c, strain compatibility, and force equilibrium, conditions can be used to formulate the following equation:

$$\left(\frac{\sum_{i=0}^{n}\sigma_{t(i)}}{n}\right)\left(\frac{A_f}{bd}\right)\left(\frac{\sum_{i=0}^{n}\sigma_{t(i)}}{nE_f} + \varepsilon_c\right) - 0.9 f_{cm}\varepsilon_c \ln\left[\frac{1 + (\varepsilon_c/\varepsilon_{cc})^2}{\varepsilon_c/\varepsilon_{cc}}\right] = 0, \tag{2}$$

where $\sigma_{t(i)}$ is the capacity of the i^{th} GFRP bar at time t (years), which is determined using equation (1). Equation (3) is only valid when the maximum concrete strain, ε_c, is less than the value of ε_{cu} and the value of c is simultaneously less than the value of $c_b = (\varepsilon_{cu} d)/(\varepsilon_{cu} + \varepsilon_{fu})$. Therefore, $\varepsilon_{\text{BF},t}(\mathbf{x}, \boldsymbol{\Theta}) = \sum_{i=0}^{n}\sigma_{t(i)}/(nE_f)$. A more detailed derivation is presented in Kim et al. [23] (see Figure 2(a)).

When the concrete crushing failure is dominant, the strain in the GFRP bar, $\varepsilon_{\text{CF},t}(\mathbf{x}, \boldsymbol{\Theta})$, can be determined using the following equation (see Figure 2(b)):

$$\varepsilon_{\text{CF},t}(\mathbf{x}, \boldsymbol{\Theta}) = 0.5\left[\varepsilon_{cu}{}^2 + \frac{4bd}{E_f A_f}\int_0^{\varepsilon_{cu}} f_{cm}(\varepsilon)d\varepsilon\right]^{0.5} - 0.5\varepsilon_{cu} \le \varepsilon_{\text{BF},t}(\mathbf{x}, \boldsymbol{\Theta}), \tag{3}$$

where the value of $\varepsilon_{\text{CF},t}(\mathbf{x}, \boldsymbol{\Theta})$ is not larger than the ultimate strain of the GFRP reinforcement, $\varepsilon_{\text{BF},t}(\mathbf{x}, \boldsymbol{\Theta})$, b is the width of the cross section (mm), d is the distance from the extreme compression fiber to the centroid of tension reinforcement (mm), A_f is the area of the GFRP reinforcement in the given section (mm^2), ε_{cu} is the concrete crushing strain in the top fiber, and E_f is the elastic modulus of GFRP reinforcement. A more detailed derivation is presented in Kim et al. [23].

3. Formulation of the Strain-Based Model (Shear)

3.1. Strength-Based Shear Capacity Model. Hoult et al.'s [36] model was calibrated based on the original modified compression field theory (MCFT) model [37]. The flexural and shear interaction was formulated with strain compatibility and equilibrium, and the model may be acceptable as long as the equation is used to design the specimen. The equation may not be applicable, however, for estimating the shear capacity of a one-way shear failure. This study, therefore, adopted constitutive equations of Hoult et al.'s model [36]. In addition, Hoult et al. [36] proposed a second-order approximation equation to capture large crack widths and excessive strain of FRP systems in concrete with respect to

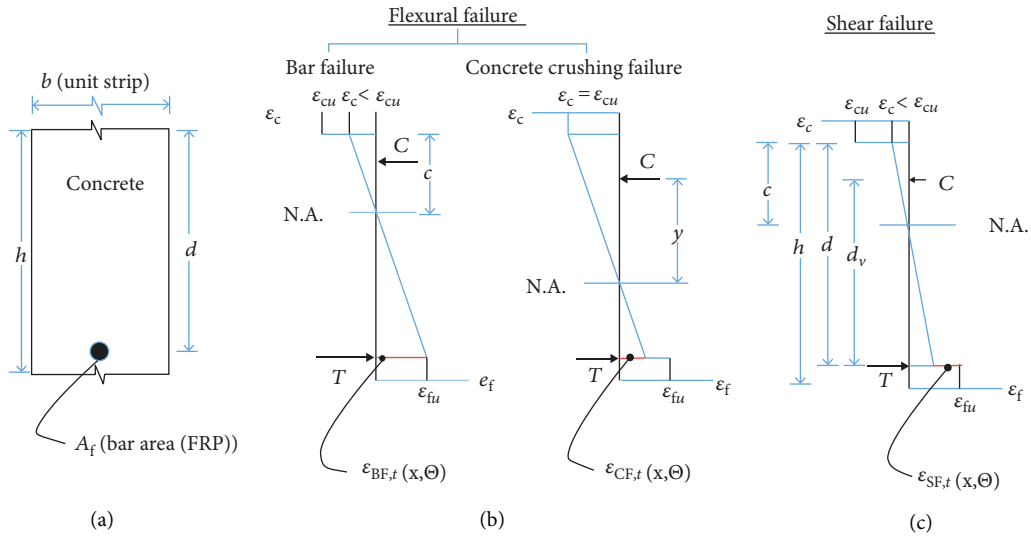

FIGURE 2: Failure modes of a bridge deck: (a) bar failure, (b) concrete crushing failure, and (c) shear failure.

shear capacity. The nominal shear capacity, $C_{SF,t}(\mathbf{x}_v)$, of the second-order equation is as follows:

$$C_{SF,t}(\mathbf{x}_v) = \frac{0.3}{0.5 + (1000\varepsilon_x + 0.15)^{0.7}} \frac{1300}{(1000 + sp_{xe})} \sqrt{f_{cm}} b_w d_v, \tag{4}$$

where ε_x is the longitudinal strain at mid-depth for predicted shear failures, b_w is the width of the web (mm), and effective crack spacing $sp_{xe} = (31.5d)/(16 + a_g) \geq 0.77d$, where a_g is the maximum aggregate size (mm). In general, the value of a_g is assumed to be 25 mm [36], f_{cm} is the compressive strength of concrete (MPa), and d_v is the effective shear depth (mm) taken as $0.9d$. The current AASHTO Bridge Design Specification [1] originated from the ACI 440.1R-06 [4]. Earlier research results indicated that the ACI 440.1R-06 model [4] underestimates shear capacity [36, 38].

3.2. Strain of GFRP Bars at Shear Failure. Hoult et al.'s model [36] is a deterministic model. To convert this model to a probabilistic model, the model error and bias-correction terms are included, based on the statistical analysis of the database collected by authors. The database includes 112 samples collected from 15 literatures [17, 18, 39–52]. Samples are FRP-reinforced beams for flexural reinforcement without shear reinforcement. The normalized shear stress, $v_n(\mathbf{x}_v)$, is as follows:

$$v_n(\mathbf{x}_v) = \frac{C_{SF,t}(\mathbf{x}_v)}{\sqrt{f_{cm}} b_w d_v} \frac{(1000 + sp_{xe})}{1300} = \frac{0.3}{0.5 + (1000\varepsilon_x + 0.15)^{0.7}} + s_v e, \tag{5}$$

where ε_x, b_w, d_v, sp_{xe}, and f_{cm} are defined in equation 4. Note that, for a given value of strain in the mid-depth of the section, the variance, $\mathrm{Var}[v_n(\mathbf{x}_v)] = s_v^2$, $s_v e$ is the model error, and e is a statistically independent, identically distributed, random variable with a mean and unit variance of zero. The variance of the model error is 0.0017. From the MCFT formulation, two equations are used: (1) $T = C_{SF,t}(\mathbf{x}_v)(a/d_v + 1)$ and (2) $\varepsilon_{SF,t}(\mathbf{x}, \boldsymbol{\Theta}) \approx 2\varepsilon_x$. The value of ε_x can be found from solving equations (5) and T, simultaneously: $\varepsilon_x = C_{SF,t}(\mathbf{x}_v)(a/d_v + 1)/(2E_f A_f)$. The variable of a/d_v indicates the moment and shear interaction to change shear and flexural capacities, depending on the truck loadings. Finally, the strain of the bar of a GFRP, $\varepsilon_{SF,t}(\mathbf{x}, \boldsymbol{\Theta})$, can be estimated based on the strain compatibility and trigonometry of the strain relationship between the bar, concrete, mid-depth strain, and neutral axis, as follows (see Figure 2(c)):

$$\varepsilon_{SF,t}(\mathbf{x}, \boldsymbol{\Theta}) = \min\left[(\varepsilon_c + \varepsilon_x)(d - c + \bar{y}) - \varepsilon_c \approx 2\varepsilon_x, \varepsilon_{BF,t}(\mathbf{x}, \boldsymbol{\Theta})\right], \tag{6}$$

where c is the distance measured from the top extreme fiber to the neutral axis, and $\bar{y}$ is the distance from the neutral axis to the location of the resultant compression force.

3.3. Formulation of the Strain-Based Capacity Model. Potential final failure mode can be determined based on the lowest strain value. When the strain of GFRP reaches the strain corresponding to failure modes, the bridge deck experiences either flexural or shear failure. The main reason to integrate both failure modes is to consider the interaction of shear and moment with respect to failure probability. Two distinct values of failure probability may provide limited information (i.e., no consideration of moment and shear interaction) and two different estimations (either flexural or shear failure). Therefore, it needs the unified reliability index that can be used as a single indicator of a representative value of failure probability. The mathematical expression of the governing

strain to determine each failure mode at time, t, can be expressed as follows:

$$SC_t(\mathbf{x}, \boldsymbol{\Theta}) = \min\left[\min\left[\varepsilon_{\mathrm{CF},t}(\mathbf{x}, \boldsymbol{\Theta}), \varepsilon_{\mathrm{BF},t}(\mathbf{x}, \boldsymbol{\Theta})\right], \varepsilon_{\mathrm{SF},t}(\mathbf{x}, \boldsymbol{\Theta})\right]. \tag{7}$$

Equation 7 consists of two terms: strain of bar corresponding to flexural failure from min $[\varepsilon_{\mathrm{CF},t}(\mathbf{x}, \boldsymbol{\Theta}), \varepsilon_{\mathrm{BF},t}(\mathbf{x}, \boldsymbol{\Theta})]$ and strain of bar corresponding to shear failure, $\varepsilon_{\mathrm{SF},t}(\mathbf{x}, \boldsymbol{\Theta})$. The minimum value will govern the final failure mode. This strain-based capacity model determined final failure over time, among multiple failure modes, with respect to strain values of GFRP reinforcement.

4. Time-Variant Demand Model

This section presents the demand model for predicting the strain of a GFPR reinforcement at a critical section. This research adopted the demand model proposed by Akgul [53].

The unfactored demand moment, $M_{\mathrm{S},t=0}(\mathbf{x}_{\mathrm{dm}})$, can be calculated as follows:

$$M_{\mathrm{S},t=0}(\mathbf{x}_{\mathrm{dm}}) = M_{\mathrm{DL}}(\mathbf{x}_{\mathrm{dm}}) + M_{\mathrm{LL}+I,t=0}(\mathbf{x}_{\mathrm{dm}}), \tag{8}$$

where $M_{\mathrm{DL}}(\mathbf{x}_{dm})$ is the dead load moment (kN-m) $(= (\lambda_{\mathrm{a}}(h_{\mathrm{a}}\gamma_{\mathrm{a}}{L_s}^2 C_{\mathrm{f}})/8) + (\lambda_{\mathrm{c}}(h_{\mathrm{s}}\gamma_{\mathrm{c}}{L_{\mathrm{s}}}^2 C_{\mathrm{f}})/8))$, $M_{\mathrm{LL}+I,t=0}(\mathbf{x}_{dm})$ is the live load moment (kN-m) $(= ((w_{\mathrm{ps}}{L_{\mathrm{s}}}^2)/8) + \lambda_{\mathrm{tr}}(L_{\mathrm{s}} + 0.6/9.75)P_{\mathrm{HS20}}C_{\mathrm{f}}I_{\mathrm{f}})$, is the statics of vectors to account for design and truck loading, h_{a} is the thickness of asphalt pavement (m), γ_{a} is the asphalt unit weight (kN/m^3), h_{s} is the thickness of concrete slab (m), w_{ps} is the uniform weight of utility piping for slab (kN/m), γ_{c} is the concrete unit weight (kN/m^3), L_{s} is the span length of the slab between two girders (m), λ_{a} is the uncertainty factor for asphalt, λ_{c} is the uncertainty factor for concrete, λ_{tr} is the uncertainty factor for truck, P_{HS20} is the load on one middle or rear wheel of an HS20 truck (71.17 kN), C_{f} is the continuity factor, and $I_{\mathrm{f}} = 1 + (15.2/L_{\mathrm{s}} + 38.1) \leq 1.3$ is the dynamic impact factor. At the specific time, t, the value of $M_{\mathrm{S},t}(\mathbf{x}_{\mathrm{dm}})$ is randomly generated from the mean and standard deviation of $M_{\mathrm{LL}+I,t=0}(\mathbf{x}_{\mathrm{dm}})$ of type I (Gumbel) distribution as a function of the cumulative number of truck traffic over time. The more trucks that cross the bridge, the higher the probability that the bridge will experience the extreme load: i.e., the change of statistical distribution from lognormal to type I (Gumbel). More derivation of calculations can be found from Akgul [53]. In this model, the number of trucks per year is assumed to be 300,000, using the assumption of 300 days/yr. It is equivalent to the average daily truck traffic (ADTT) of 1000. Similarly, the strain of service moment, $SD_t(\mathbf{x})$, can be expressed as follows:

$$SD_t(\mathbf{x}) = \frac{M_{\mathrm{S},t}(\mathbf{x}_{dm})}{[E_{\mathrm{f}}A_{\mathrm{f}}(1 - k/3)d]}, \tag{9}$$

where k is the ratio of neutral axis to reinforcement depth (ACI 440.1R, Eq. (7.3.2.2b)). In this study, all the sections are assumed to be cracked, indicating the initial crack width, which is greater than zero.

5. Parametric Study on Design Cases

5.1. General. The proposed formulation was used to estimate the probability of failure of various GFRP-reinforced bridge decks that were designed in accordance with AASHTO specifications [1, 2]. Table 1 summarizes the statistical properties of deck concrete and GFRP bars, in order to estimate the flexural and shear capacities of a bridge deck. The asphalt thickness was assumed to be 50 mm. The deck thickness and cover depth were assumed to be random variables. Distribution, mean, and standard deviations were obtained from previous studies of steel-reinforced concrete bridge decks. In this study, the shear span length was treated as a random variable. The mean is the wheel at the midspan (equal to half of the girder spacing), and the standard deviation is assumed as the difference between the shear span at midspan and the possible lowest value of shear span length corresponding to $a/d = 2.5$. For example, it yields a mean of 1.2 m and standard deviation of 0.72 m for the girder spacing of 2.4 m. A mean and standard deviation for different girder spacings (1.8 and 3.7 m) are also presented in Table 1.

Table 2 shows a total of seven design cases. The main variables of design cases are the combinations of girder spacing (first number in the case I.D.) and the thickness of the deck (second number of case I.D.). The combinations originated from the selection of the typical range of steel-reinforced bridge decks [59]. The ratio of the provided GFRP reinforcement, ρ_{f}, to the balanced GFRP reinforcement, $(\rho_{\mathrm{f}}/\rho_{\mathrm{fb}})$, was assumed to be 1.82, which allowed the maximum crack width below the allowable maximum crack width of 0.5 mm. The maximum crack width can be calculated from the AASHTO LRFD specifications [1]. In addition, ACI 440.1R-15 [6] reported that typical ratio, $\rho_{\mathrm{f}}/\rho_{\mathrm{fb}}$, is assumed to be 2.0 for the slab to meet the deflection limit, $l/240$ [6]. The mean maximum crack widths are presented in the sixth column of Table 2. To achieve the equal reinforcement ratio, six design cases were planned, using M13. One design case (considered as a benchmark design case) was designed, using M19 to investigate the bar size effect.

Table 3 shows the properties of M13 and M19 GFRP-reinforcing bars. Statistical distributions are assumed to be lognormal for diameter, elastic modulus, mean capacity, and diffusion coefficient of bars. Due to the lack of information on GFRP-reinforced bridge deck designs, the authors assumed that the selected design combinations of deck thickness and girder spacing can be applicable to the design of GFRP-reinforced bridge decks.

The temperature range is determined based on the mean values of annual temperatures in the US territories. The actual fluctuation of exposure temperatures is much greater than three constant values. In general, the lowest temperature (13 °C) represents the average exposure temperature of the cold regions, while the highest temperature (33 °C) represents the average temperature of the warm region. The reference temperature (23°C) were used to develop the model in the

Table 1: Parameters of deck design and uncertainties of demand.

Parameter	Mean	Standard deviation	COV	Distribution	Descriptions	Source
f_{cm} (MPa) 27.5	$1.24f_c'$ 34.1	6.34	0.15	Lognormal	Compressive strength	[21]
v_o (mm)	38.1	1.9	0.05	Lognormal	Clear cover	[54]
h_s (mm)	Varied (μ)	3.96	1/(6.4 μ)	Normal	Concrete deck depth	[55]
d (mm)	$0.99d_n$	—	0.04	Normal	Effective depth	[56]
a_g (mm)	25	N.A.	N.A.	Deterministic	Max. aggregate size	[36]
d_v (mm)	$d_v = 0.9d$	N.A.	N.A.	Normal	Shear effective depth	[57]
λ_a	1.0	0.25	—	Lognormal	Uncertainty factor for asphalt weight	[58]
λ_c	1.05	0.11	—	Lognormal	Uncertainty factor for concrete weight	
λ_{tr}	0.60	0.20	—	Lognormal	Uncertainty factor for truck	
C_f	0.8	—	—	Deterministic	Continuity factor	
h_a (mm)	50	—	—	Deterministic	Asphalt thickness	
L_s, (m)	2.36	—	—	Deterministic	Span length of slab	
P_{HS20} (kN)	71.17	—	—	Deterministic	Wheel load of HS 20 truck	
a, m (ft.)	0.9	0.56	0.61	Lognormal	Shear span for girder spacing (1.8 m)	Authors' assumption
	1.2	0.72			Shear span for girder spacing (2.4 m)	
	1.8	1.12			Shear span for girder spacing (3.7 m)	

Note: d_n = nominal effective depth

Table 2: Conventional deck design.

Case I.D.	Girder spacing (m)	Deck thickness (mm)	Number of bars—bar size (metric)	Spacing, (mm)	Mean max. crack width, mm ($t = 0$)	ρ_f/ρ_{fb}	$M_{S,t=0}(\mathbf{x}_{dm})$ (kN-m/m) Mean	Std.
1.8-180-13	1.8	180	3.13 - M13	97	0.43	1.82	12.97	3.72
1.8-200-13		200	3.73 - M13	82	0.27	1.82	13.18	3.68
2.4-230-13	2.4	230	4.33 - M13	70	0.23	1.82	17.32	4.63
2.4-230-19	2.4	230	1.92 - M19	158	0.11	1.82	17.32	4.63
3.7-200-13	3.7	200	3.73 - M13	82	0.50	1.82	27.68	6.46
3.7-230-13		230	4.33 - M13	70	0.38	1.82	28.46	6.46
3.7-250-13		250	4.92 - M13	62	0.27	1.82	29.50	6.59

previous research of the author in Texas region [34]. Much information on the temperature effect is available in [34].

It should be noted that the current study focuses on the application of GFRP reinforcement in bridge structures. When the data from carbon fiber reinforced polymer (CFRP) is available, the proposed methodology can be applied to the deterioration model of CFRP in concrete, in which CFRP is more durable and exhibited high strength and high stiffness in general. As the application of CFRP gains more popularity in the field of infrastructure construction, it is expected that the experimental data and reliability analysis would be readily available, which will lead to the application of the proposed approach to various composite materials for improvement of the system reliability in near future.

5.2. Safety Margin. Using the probabilistic model for the time-variant strain capacity of the GFRP deck described in equation (8), the limit state function can be expressed as $g_t(\mathbf{x}, \boldsymbol{\Theta}) = SC_t(\mathbf{x}, \boldsymbol{\Theta}) - SD_t(\mathbf{x})$. The safety margin is formulated as the limit state function and the difference between capacity (equation (7)) and demand (equation (9)). When the value of the safety margin is greater than zero, the designed deck is safe. Conversely, a negative value indicates that the designed deck is unsafe. In the manner of physical interpretation, the value of zero indicates that the average strain of GFRP bars reached the one particular failure strain value $[\varepsilon_{CF,t}(\mathbf{x}, \boldsymbol{\Theta}), \varepsilon_{BF,t}(\mathbf{x}, \boldsymbol{\Theta}), \varepsilon_{SF,t}(\mathbf{x}, \boldsymbol{\Theta})]$. Figure 3 shows the safety margin of two design cases of 1.8-180 and 2.4-230. Mean (μ), and mean ± standard deviations ($\mu \pm \sigma$) of safety margin (herein, expressed as an average strain value of GFRP bars) are shown plotted over different exposure times (0, 0.5, 2.5, 5, 10, 15, 25, 50, and 75 years). The safety margin presented marginal strains of GFRP bars ranging from 0.46×10^{-3} ($[\mu - \sigma]$ in the design case of 1.8-180-13 at 75 years) to 7.34×10^{-3} ($[\mu + \sigma]$ in the design case of 2.4-230-13 at 0 year). In general, the safety margin significantly reduced from 0 year to 0.5 year. The design case of 1.8-180-13 exhibited a lower safety margin compared to that of 2.4-230-13.

Table 3: Parameters of GFRP reinforcement.

Bar size	Parameter	Mean	Standard deviation	Distribution	Descriptions	Source
M13	r (mm)	6.35	0.76	Lognormal	Radius	[34]
	E_f (MPa)	46,263	5212	Lognormal	Modulus of elasticity	[34]
	$\mu_{\sigma 0}$ (MPa)	779	*25	Lognormal	Mean capacity at $t = 0$	* [60]
	D_{T23} (m^2/sec)	8.903×10^{-13}	3.522×10^{-13}	Lognormal	Diffusion coeff.	[34]
M19	r (mm)	9.53	1.14	Lognormal	Radius	[34]
	E_f (MPa)	47,573	5357	Lognormal	Modulus of elasticity	[34]
	$\mu_{\sigma 0}$ (MPa)	696	14	Lognormal	Mean capacity at $t = 0$	[34]
	D_{T23} (m^2/sec)	8.903×10^{-13}	3.522×10^{-13}	Lognormal	Diffusion coeff.	[34]

Note: asterisks indicate the source of standard deviation.

This indicates that the design of 1.8-180-13 has higher probability of failure over time. The significant reduction in the safety margin of the 1.8-180-13 design case was observed from 0 to 0.5 year. Beyond a 0.5-year exposure, the overtime reduction rate of the two design cases exhibited similarly for μ and $\mu \pm \sigma$ plots.

6. Time-Variant Reliability

6.1. General. The time-variant reliability index, $\beta(t)$, is determined as the inverse of the standard normal cumulative distribution as a function of exposure time, t: $\beta(t) = -\Phi^{-1}(P_f(t))$, where Φ^{-1} is the inverse standard normal distribution function and the probability of failure, $P_f(t)$, can be estimated from the following equation at the given time, t: $P_f(t) = P(g_t(\mathbf{x}, \boldsymbol{\Theta}) < 0)$. Both are convenient indications of the safety of the structural components [61]. In this paper, the focus is on reliability indices. A total of 3×10^6 Monte Carlo simulations per each exposure time were undertaken to estimate the probability of failure in GFRP-reinforced bridge decks. The simulation terminated when the target coefficient of variation of failure probability reached 0.01, before reaching maximum simulations.

In this study, the initial reliability indices were calculated at $t = 0$, assuming the value of $C_E = 1.0$. The current practice of reliability analysis assumes that the single value of the reduction factor has been used, regardless of the degradation condition. As discussed earlier, the failure mode can be potentially changed over time even though the section is initially designed as a compression-controlled section. The probability of failure recommended by the AASHTO Load and Resistance Factor Rating (LRFR) [62] is $6.21^\circ \times {}^\circ 10^{-3}$, corresponding to the reliability index, $\beta(t)$ of 2.5 at the service. When the reliability index is lower than 2.5, this indicates that the GFRP-reinforced bridge deck exhibits high risk of any type of failure beyond the specific exposure time.

6.2. Integration of Multiple Failure Modes. Figure 4 shows reliability indices of two design cases subjected to three different exposure temperatures.

Time-variant reliability indices of flexural failure, shear failure, and integrated two-failure modes (using equation (7), designated as total) are presented. In general, the probability of failure increases dramatically at the early age of exposure, as observed in the safety margin. Within one year, the bar capacity reduced significantly with the increase in the demand, dramatically impacting the reduction of the reliability index. Higher temperatures significantly increased the probability of failure over time, as shown in Figure 4(a) versus 4(b). To understand how the dominancy of failure mode changed over time, reliability indices of flexural and shear failure were compared over time. Among all the design cases in this study, the β value of flexural failure (red line with closed circle) generally exhibited high sensitivity to the exposure time, resulting in the change of the β value of integrated failure modes (blue line with open circle).

The maximum service life is defined as the time required to reach the reliability index of 2.5 (black line, designated as LRFR [62]). It should be noted that the definition can be varied, depending on the researchers' and engineers' perspectives of the expected performance. In this study, the authors focused on the probability of failure over time. A time to reach the value of 2.5 can be determined from the intersection between two lines, LRFR [62] and estimated reliability indices.

Design parameters, such as girder spacing and deck thickness, influence the dominancy of failure mode at the initial design. For example, the design cases of 1.8-180-13 and 3.7-250-13 were compared with respect to failure dominancy. In one, the shear failure mode affected the overall failure probability (hereafter, reliability index); in the other, the flexural mode affected the overall failure probability. However, exposure temperature altered the dominancy of failure mode over time. In the design case of 1.8-180-13, shear failure (green line with star) dominantly controlled the failure probability, as shown in Figure 4(b, i). As the exposure time and temperature increased, the flexural failure mode took over the shear failure mode. The reliability index of shear failure is not governed by the exposure temperature, but the exposure temperature does play an important role in determining the reliability indices of flexural failure. This led to an increase in the overall failure probability in all the design cases. The impact of exposure temperature is discussed in the following section.

Integrated failure mode and its time-variant reliability are dependent not only on exposure time but also on exposure temperature. This tendency is clearly observed in the 1.8-180-13 design case, when flexural and shear failure modes

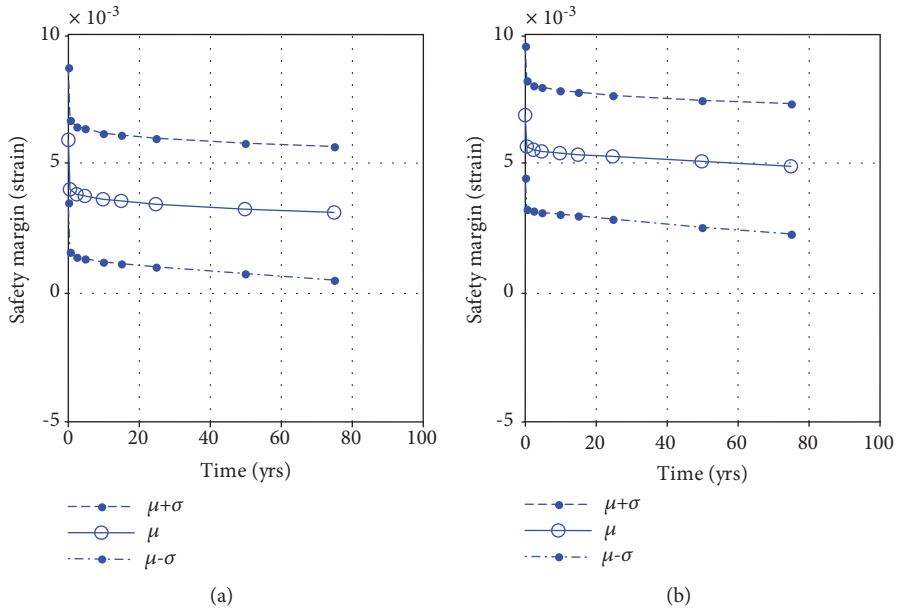

Figure 3: Typical plot of safety margin: (a) 1.8-180-13 and (b) 2.4-230-13.

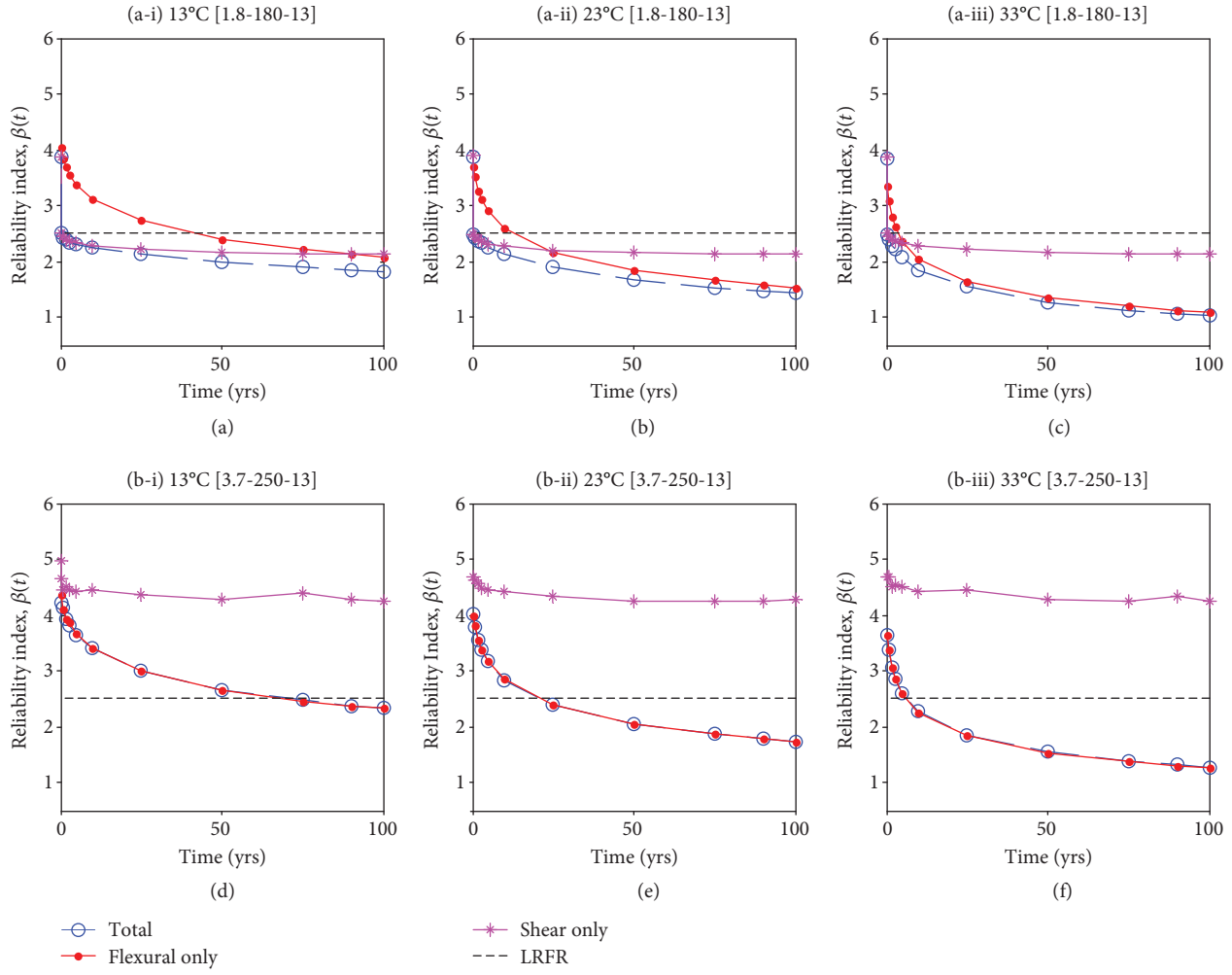

Figure 4: Time-variant reliability index: flexural, shear, flexural, and shear (total): (a, i) 13°C [1.8-180-13], (a, ii) 23°C [1.8-180-13], (a, iii) 23°C [1.8-180-13], (b, i) 13°C [3.7-250-13], (b, ii) 23°C [3.7-250-13], and (b, iii) 23°C [3.7-250-13].

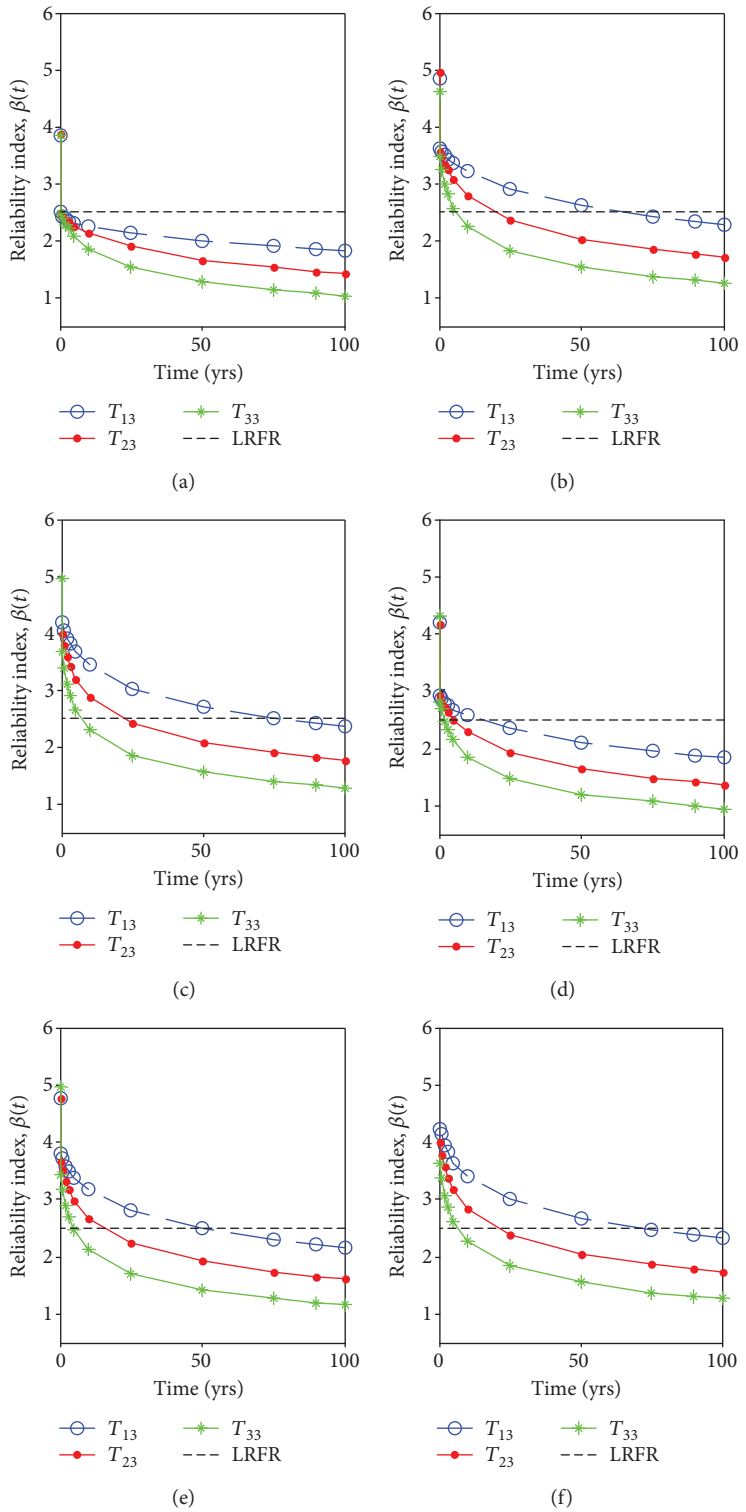

Figure 5: Effect of exposure temperature of 13, 23, and 33°C: (a) 1.8-180-13, (b) 1.8-200-13, (c) 2.4-230-13, (d) 3.7-200-13, (e) 3.7-230-13, and (f) 3.7-250-13.

yield closer values of reliability indices. This seems to capture both risks of failure, exhibiting lower reliability indices than the individual values obtained from each failure mode. When one typical failure (typically, the flexural failure) governs the overall failure mode, the reliability indices are determined by the governed failure mode. Therefore, the proposed limit state function provides the rational estimation, using Monte Carlo simulations.

6.3. Temperature Effect. Figure 5 shows the time-variant reliability indices of all the design cases subjected to the constant exposure temperature. The three exposure temperatures

Table 4: Time-variant reliability indices, $\beta(t)$ (six design cases: only M13).

Case	Girder spacing, (m)	Deck thickness mm (in.)	13°C		23°C		33°C	
			$\beta(t=0)$ (0 years)	$\beta(t=100)$ (100 years)	$\beta(t=0)$ (0 years)	$\beta(t=100)$ (100 years)	$\beta(t=0)$ (0 years)	$\beta(t=100)$ (100 years)
1.8-180-13	1.8	180	3.86	1.82	3.88	1.43	3.84	1.04
1.8-200-13		200	4.83	2.29	4.97	1.72	4.61	1.26
2.4-230-13	2.4	230	>4.97	2.36	>4.97	1.77	4.97	1.29
3.7-200-13		200	4.19	1.85	4.18	1.37	4.31	0.93
3.7-230-13	3.7	230	4.75	2.17	4.75	1.61	4.97	1.15
3.7-250-13		250	>4.97	2.33	>4.97	1.74	>4.97	1.27
Avg.			4.60	2.13	4.62	1.61	4.61	1.16
Std.			0.42	0.22	0.43	0.16	0.42	0.13
COV			0.09	0.10	0.09	0.10	0.09	0.12

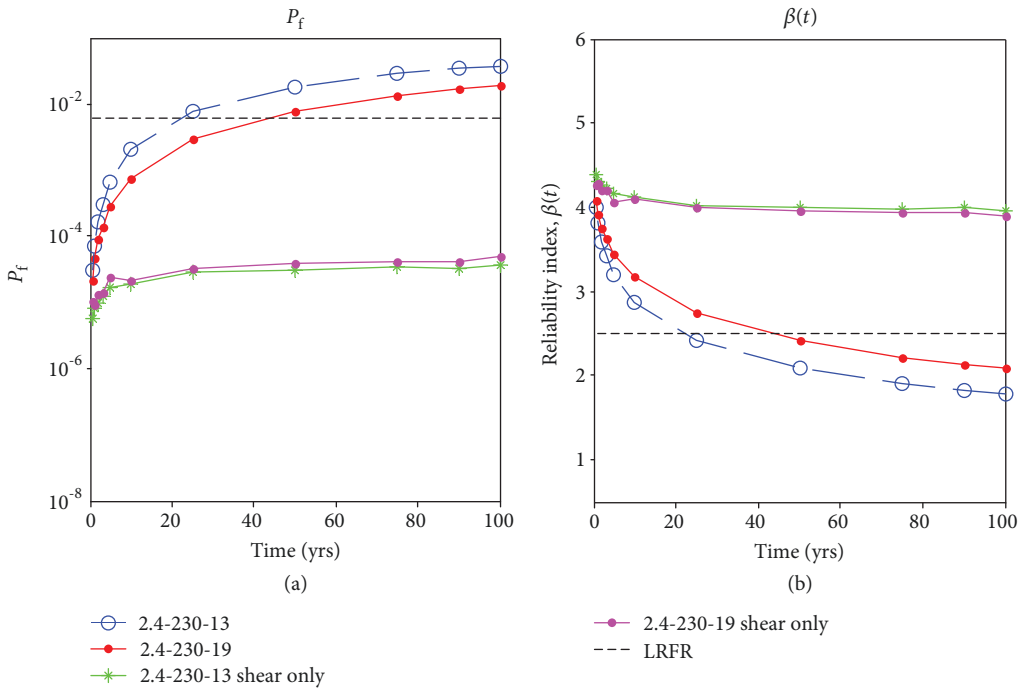

Figure 6: Failure probability and reliability index (bar size effect).

were 13°C (designated as T_{13}), 23°C (designated as T_{23}), and 33°C (designated as T_{33}). All the design cases of 33°C exposure temperature reached the target reliability index of 2.5 after only a few years. Before 10 years of exposure to high temperatures, all the design cases exceeded the probability of failure recommended by AASHTO LRFR [62]. The exposure temperature of 33°C changed the reliability index governed by the reduction of reliability index of flexural failure. Similarly, a low temperature of 13°C decelerated the progress of flexural failure over time, resulting in the extension of time to reach the acceptable reliability index (i.e., the extension of service life). In general, the girder design of 3.7-250-13 exhibited the lowest reliability index after 100 years. As the thickness of the bridge deck increases, the reliability indices increase (see Figures 5(d)–5(f)). However, the highest reliability index at low temperature (13°C) of 3.7-200-13 exhibited a higher value compared to the lowest reliability index at high temperature (33°C) of 3.7-250-13 (see Figure 5(d): T_{13} versus Figure 5(f): T_{33}). This indicates that exposure temperature is a more significant contributor than the design parameter of deck thickness. Figures 5(b) and 5(d) show that the deck having a shorter girder spacing generally exhibited lower reliability indices in the same exposure temperature, while the design case of 1.8-200-13 of 33°C (T_{33}) exhibited a similar risk to the design case of 3.7-200-13 at 23°C (T_{23}) (see Figure 5(b): T_{33} versus Figure 5(d): T_{23}).

Table 4 shows the summary of reliability indices at 0 and 100 years for design cases containing M13 bars. The reliability index of the initial design ranged from 3.84 to greater than 4.97 in all of the design cases. Shortening girder spacing can mitigate the risk of failure when the same deck thickness is

used (e.g., 1.8-200-13 versus 3.7-200-13). The various combinations of deck thickness and girder spacing affect the reliability index. For example, a 50 mm increase in deck thickness increases the reliability index of 100 years from 26 to 37% (3.7-200-13 versus 3.7-250-13). The increase in girder spacing decreases the reliability index at 100 years from 24 to 35% (1.8-200-13 versus 3.7-200-13). At the initial time $(t = 0)$, an average of the reliability index was estimated to be 4.61 (see Table 4). After 100 years, as the exposure temperature increases from 13 to 33°C, the reliability indices decrease, ranging from 43 to 50%. Therefore, the exposure temperature is more important than any other design parameter.

6.4. Bar Size Effect. Figures 6 (a) and (b) show the failure probability and reliability indicies of the design case of 2.4-230, with two different bar sizes: M13 and M19.

They were exposed to a standard temperature of 23°C. As the size of the bar increased, the probability of failure decreased. In addition, the time to reach the reliability index of 2.5 extended from about 25 to 50 years. This concurs with a similar trend in analytical results [23]. In this study, it was not found that the bar size effect was related to estimating reliability indices associated with shear failure.

7. Conclusion

In this study, a reliability analysis framework is proposed for glass fiber-reinforced polymer- (GFRP-) reinforced concrete systems with uncertain capacities and demands over time. This is the first attempt to integrate the flexural and shear failure modes for GFRP-reinforced concrete members in a single analysis framework. A total of seven typical configurations of bridge decks with a variety of deck thicknesses and girder spacing were investigated. These different configurations changed the demand as well. Six design cases with M13 bars were exposed to three different temperatures (13, 23, and 33°C). The ratio of the provided GFRP reinforcement, ρ_f, to the balanced GFRP reinforcement, (ρ_f/ρ_{fb}), was determined to be 1.82 to meet the serviceability requirement. One design case contained M19 bars, with the same bar ratio of M13 bars. The following findings and conclusions may be drawn:

(1) The various combinations of deck thickness and girder spacing affect the reliability index. The safety margins and reliability indices dramatically decrease at an early age (i.e., 0 to 0.5 years). This is attributed to the increase in demand and the reduction in flexural capacity. The reliability index of shear failures is mainly affected by the change of demand, rather than exposure temperature

(2) The proposed limit state function provides rational estimation, with the likelihood of capturing flexural and shear failure modes, simultaneously

(3) The reliability indices of 100 years of exposure exhibited significant variances, ranging from 2.35 to 0.93 in the exposure temperatures ranging from 13°C to 33°C. The simulation results show that all the design cases exhibited lower than the target reliability index of 2.5 recommended by AASHTO LRFR after 100 years of exposure

(4) In general, as exposure time and temperature increase, the flexural failure affects the determination of overall reliability indices. In a bridge deck having a thin thickness and short girder spacing, shear failure tends to affect the overall reliability index, resulting in a high probability of failure (i.e., low reliability index).

(5) In the benchmark design case, the increase in the bar size could be an alternative for extending the service life. From these simulations, the M19 bar increased the service life approximately 100% to reach the target reliability index of 2.5

In summary, exposure temperatures dramatically affect the service life (e.g., expectancy of life to reach the specific target reliability index). The change in the reliability index is more sensitive (i.e., more changes) with exposure to higher temperatures. Therefore, further experimental and analytical research is needed on both deck configuration and exposure temperature of the GFRP-reinforced bridge deck exposed to high temperatures.

Notations

A_f: The area of the GFRP reinforcement in the given section (mm^2)
a_g: Maximum aggregate size (mm)
b: The width of the cross section (mm)
b_w: The width of the web (mm), effective crack spacing
c_b: $(\varepsilon_{cu}d)/(\varepsilon_{cu} + \varepsilon_{fu})$, the depth of neutral axis
C_f: Continuity factor, and dynamic impact factor
$C_{CF,t}(\mathbf{x}, \boldsymbol{\Theta})$: The nominal moment capacity of concrete crushing failure
$C_{BF,t}(\mathbf{x}, \boldsymbol{\Theta})$: The nominal moment capacity of bar failure
$D_{T_{23}}$: The diffusion coefficient at a defined reference temperature (23°C)
d: The distance from the extreme compression fiber to the centroid of tension reinforcement (mm)
d_v: The effective shear depth (mm) taken as $0.9d$
E_a: The activation energy (KJ)
E_f: The elastic modulus of GFRP reinforcement
e_0, e: Statistically independent, identically distributed random variables with a mean and unit variance of zero
f_{cm}: The compressive strength of concrete (MPa)
$f_{fu}^* = f_{fu,ave} - 3\sigma$: Guaranteed tensile strength of GFRP reinforcement
$f_{fu,ave}$: The mean tensile strength of sample of test specimens
h_a: Thickness of asphalt pavement (m)
h_s: Thickness of concrete slab (m)

I_f: $1 + (15.2/L_s + 38.1) \le 1.3$ at the specific time, t
k: The ratio of neutral axis to reinforcement depth (ACI 440.1R, Eq. (7.3.2.2b))
L_s: The span length of the slab between two girders (m)
$M_{DL}(\mathbf{x}_{dm})$: The dead load moment $(= (\lambda_a(h_a\gamma_a L_s{}^2 C_f)/8) + (\lambda_c(h_s\gamma_c L_s{}^2 C_f)/8))$ (kN-m)
$M_{LL+I,t=0}(\mathbf{x}_{dm})$: The live load moment $(= (w_{ps}L_s{}^2)/8 + \lambda_{tr}(L_s + 0.6/9.75)P_{HS20}C_f I_f)$ (kN-m)
$M_{S,t}(\mathbf{x}_{dm})$: Randomly generated from mean and standard deviation of $M_{LL+I,t=0}(\mathbf{x}_{dm})$ of type I (Gumbel) distribution as a function of cumulative number of truck traffic over time
s_0, s, s_v: The standard deviations of the error terms, $s_0 e_0$, se, and $s_v e$, respectively
P_{HS20}: The load on one middle or rear wheel of an HS20 truck
$P_f(t)$: The following equation at the given time, t: $P_f(t) = P(g_t(\mathbf{x}, \boldsymbol{\Theta}) < 0)$
R: The universal gas constant (KJ/mol-K)
r: The radius of the GFRP reinforcement
$SD_t(\mathbf{x})$: The strain of service moment
sp_{xe}: Effective crack spacing $(= (31.5d)/(16 + a_g) \ge 0.77d)$
T_{23}: 296 K (23°C)
T: The exposure temperatures (in K)
$v_n(\mathbf{x}_v)$: Normalized shear stress
w_{ps}: Uniform weight of utility piping for slab (kN/m)
σ: Standard deviation
$\sigma_{t(i)}$: Capacity of the i^{th} GFRP bar at time t (years)
$\beta(t)$: Time-variant reliability index, $\beta(t) = -\Phi^{-1}(P_f(t))$
γ_a: Asphalt unit weight (kN/m^3)
γ_c: Concrete unit weight (kN/m^3)
ε_{cu}: Concrete crushing strain in the top fiber
ε_x: Longitudinal strain at mid-depth for predicted shear failures
$\varepsilon_{BF,t}(\mathbf{x}, \boldsymbol{\Theta})$: Corresponding strain of bar failure
$\varepsilon_{CF,t}(\mathbf{x}, \boldsymbol{\Theta})$: Corresponding strain of concrete crushing failure
$\varepsilon_{SF,t}(\mathbf{x}, \boldsymbol{\Theta})$: Corresponding strain of shear failure
$\boldsymbol{\Theta}$: Vectors to capture the parameters, $\mathbf{x}$ to estimate nominal moment capacities
$\boldsymbol{\Theta}_\sigma$: A vector of unknown parameters introduced to fit the data
$\boldsymbol{\Theta}_E$: A vector of unknown parameters to fit the data of elasticity of concrete
λ_a: Uncertainty factor for asphalt
λ_c: Uncertainty factor for concrete
λ_{tr}: Uncertainty factor for truck
μ_{σ_0}: Mean tensile strength of sample of test specimens
Φ^{-1}: The inverse standard normal distribution function and the probability of failure
$\mathbf{x}$: Vectors of parameters
$\mathbf{x}_b$: A vector of basic variables for bar properties
$\mathbf{x}_v$: A vector of basic variables for shear
$\mathbf{x}_{dm}$: A vector of demand.

Data Availability

The data set is generated by Monte Carlo simulation for this study's outcomes. Therefore, the data set can be created by any researchers when Tables 2 and 3 are available.

Conflicts of Interest

The authors declare that there is no conflict of interest regarding the publication of this paper.

Acknowledgments

The authors wish to express gratitude and sincere appreciation of the partial financial support by the University of Louisville.

References

[1] AASHTO, *AASHTO LRFD Bridge Design Guide Specifications for GFRP-Reinforced Concrete Bridge Decks and Traffic Railings*, p. 68, 2009.
[2] AASHTO, *AASHTO LRFD Bridge Design Specification, Interim Revision*, Washington, DC, 2010.
[3] CSA, *Canadian Highway Bridge Design Code. CSA Standard CAN/CSA-S6-06*, Canadian Standards Association, 2006.
[4] ACI Committee 440, *Report on Fiber-Reinforced Polymer (FRP) Reinforcement for Concrete Structures*, 2006.
[5] ACI Committee 440, *Report on Fiber-Reinforced Polymer (FRP) Reinforcement for Concrete Structures*, 2008.
[6] ACI Committee 440, *ACI 440.1R-15 Guide for the Design and Construction of Structural Concrete Reinforced with Fiber-Reinforced Polymer (FRP) Bars*, 2015.
[7] R. V. Rodrigues, A. Muttoni, and M. F. Ruiz, "Influence of shear on rotation capacity of reinforced concrete members without shear reinforcement," *ACI Structural Journal*, vol. 107, no. 5, pp. 516–525, 2010.
[8] A. Muttoni and M. Fernandez Ruiz, "Shear strength of members without transverse reinforcement as function of critical shear crack width," *ACI Structural Journal*, vol. 105, no. 2, pp. 163–172, 2008.
[9] B. Hu and Y.-F. Wu, "Effect of shear span-to-depth ratio on shear strength components of RC beams," *Engineering Structures*, vol. 168, pp. 770–783, 2018.
[10] B. Hu and Y.-F. Wu, "Quantification of shear cracking in reinforced concrete beams," *Engineering Structures*, vol. 147, pp. 666–678, 2017.
[11] Y.-F. Wu and B. Hu, "Shear strength components in reinforced concrete members," *Journal of Structural Engineering*, vol. 143, no. 9, article 4017092, 2017.
[12] Y. Zhou, M. Guo, L. Sui et al., "Shear strength components of adjustable hybrid bonded CFRP shear-strengthened RC beams," *Composites Part B: Engineering*, vol. 163, pp. 36–51, 2019.

[13] K.-K. Choi and H.-G. Park, "Unified shear strength model for reinforced concrete beams—part II: verification and simplified method," *ACI Structural Journal*, vol. 104, no. 2, pp. 153–161, 2007.

[14] H.-G. Park, S. Kang, and K.-K. Choi, "Analytical model for shear strength of ordinary and prestressed concrete beams," *Engineering Structures*, vol. 46, pp. 94–103, 2013.

[15] K.-K. Choi, J.-C. Kim, and H.-G. Park, "Shear strength model of concrete beams based on compression zone failure mechanism," *ACI Structural Journal*, vol. 113, no. 5, pp. 1095–1106, 2016.

[16] K.-K. Choi, W. C. Sim, J. C. Kim, and H. G. Park, "Maximum shear strength of slender RC beams with rectangular cross sections," *Journal of Structural Engineering*, vol. 141, no. 7, article 4014184, 2015.

[17] A. K. El-Sayed, E. F. El-Salakawy, and B. Benmokrane, "Shear strength of FRP-reinforced concrete beams without transverse reinforcement," *ACI Structural Journal*, vol. 103, no. 2, pp. 235–243, 2006.

[18] A. F. Ashour, "Flexural and shear capacities of concrete beams reinforced with GFRP bars," *Construction and Building Materials*, vol. 20, no. 10, pp. 1005–1015, 2006.

[19] R. D. Amico, *Shear Strength and Strength Degradation of Concrete Bridge Decks with GFRP Top Mat Reinforcement, in Civil Engineering*, Virginia polytechnic institute and State University, 2006.

[20] T. K. Hassan and S. H. Rizjalla, "Punching shear strength of GFRP reinforced deck slabs in slab-girder bridges," in *4th International Conference on Advanced Composite Materials in Bridges and Structures*, Calgary, Alberta, 2004.

[21] A. S. Nowak and M. M. Szerszen, "Calibration of design code for buildings (ACI 318): part 1—statistical models for resistance," *ACI Structural Journal*, vol. 100, no. 3, pp. 377–382, 2003.

[22] C. K. Shield, T. V. Galambos, and P. Gulbrandsen, *On the History and Reliability of Flexural Strength of FRP Reinforced Concrete Members in ACI 440.1R*, R. S. R. Sen, C. Shield, and W. Gold, Eds., American Concrete Institute, Farmington Hills, MI, USA, 2011.

[23] Y. H. Kim, D. Trejo, and P. Gardoni, "Time-variant reliability analysis and flexural design of GFRP-reinforced bridge decks," *Journal of Composites for Construction*, vol. 16, no. 4, pp. 359–370, 2012.

[24] M. M. Flint, J. W. Baker, and S. L. Billington, "A modular framework for performance-based durability engineering: from exposure to impacts," *Structural Safety*, vol. 50, pp. 78–93, 2014.

[25] F. E. Tannous and H. Saadatmanesh, "Environmental effects on the mechanical properties of E-glass FRP rebars," *ACI Materials Journal*, vol. 95, no. 2, pp. 87–100, 1998.

[26] D. Trejo, F. Aguiñiga, R. L. Yuan, R. W. James, and P. B. Keating, *Characterization of Design Parameters for Fiber Reinforced Polymer Composite Reinforced Concrete Systems*, Tech. Rep. 9-1520-3, Texas Transportation Institute Research Report, 2005.

[27] A. Mukherjee and S. J. Arwikar, "Performance of glass fiber-reinforced polymer reinforcing bars in tropical environments - part I: structural scale tests," *ACI Structural Journal*, vol. 102, no. 5, pp. 745–753, 2005.

[28] A. A. Mufti, N. Banthia, B. Benmokrane, M. Boulfiza, and J. P. Newhook, "Durability of GFRP composite rods," *Concrete International*, vol. 29, no. 2, pp. 37–42, 2007.

[29] A. A. Mufti, M. Onofrei, B. Benmokrane et al., "Field study of glass-fibre-reinforced polymer durability in concrete," *Canadian Journal of Civil Engineering*, vol. 34, no. 3, pp. 355–366, 2007.

[30] B. Benmokrane and P. Cousin, *University of Sherbrook GFRP Durability Study Report*, Intelligent Sensing for Innovative Structures (ISIS), Winnipeg, MB, Canada, 2005.

[31] A. S. M. Kamal and M. Boulfiza, "Durability of GFRP rebars in simulated concrete solutions under accelerated aging conditions," *Journal of Composites for Construction*, vol. 15, no. 4, pp. 473–481, 2012.

[32] B. Benmokrane, P. Wang, T. Pavate, and M. Robert, "Durability of FRP composites for civil infrastructure applications," in *Durability of Materials and Structures in Building and Civil Engineering*, C. W. Yu and J. W. Bull, Eds., Whittles Publishing, Dunbeath, Scotland, 2006.

[33] Y. Park, Y. Kim, and S.-H. Lee, "Long-term flexural behaviors of GFRP reinforced concrete beams exposed to accelerated aging exposure conditions," *Polymers*, vol. 6, no. 6, pp. 1773–1793, 2014.

[34] P. Gardoni, D. Trejo, and Y. H. Kim, "Time-variant strength capacity model for GFRP bars embedded in concrete," *Journal of Engineering Mechanics*, vol. 139, no. 10, pp. 1435–1445, 2013.

[35] P. Gardoni, K. M. Nemati, and T. Noguchi, "Bayesian statistical framework to construct probabilistic models for the elastic modulus of concrete," *Journal of Materials in Civil Engineering*, vol. 19, no. 10, pp. 898–905, 2007.

[36] N. A. Hoult, E. G. Sherwood, E. C. Bentz, and M. P. Collins, "Does the use of FRP reinforcement change the one-way shear behavior of reinforced concrete slabs?," *Journal of Composites for Construction*, vol. 12, no. 2, pp. 125–133, 2008.

[37] E. C. Bentz, F. J. Vecchio, and M. Collins, "Simplified modified compression field theory for calculating shear strength of reinforced concrete elements," *ACI Structural Journal*, vol. 103, no. 4, pp. 614–624, 2006.

[38] E. A. Ahmed, E. F. el-Salakawy, and B. Benmokrane, "Shear performance of RC bridge girders reinforced with carbon FRP stirrups," *Journal of Bridge Engineering*, vol. 15, no. 1, pp. 44–54, 2010.

[39] T. Alkhrdaji, M. A. Wideman, A. Belarbi, and A. Nanni, "Shear strength of GFRP RC beams and slabs," in *Proceedings of CCC 2001, Composites in Construction*, pp. 409–414, Porto, Portugal, 2001.

[40] D. H. Deitz, I. E. Harik, and H. Gesund, "One-way slabs reinforced with glass fiber reinforced polymer reinforcing bars," in *Proceedings of 4th International Symposium on Fiber reinforced polymer reinforcement for Rein-forced concrete structures*, Baltimore: American Concrete Institute, 1999.

[41] N. Duranovic, K. Pilakoutas, and P. Waldron, "Tests on concrete beams reinfored with glass fiber reinforced plastic bars," in *FRPRCS-3*, Japan Concrete Institute, Sapporo, Japan, 1997.

[42] A. K. El-Sayed, E. F. El-Salakawy, and B. Benmokrane, "Shear capacity of high-strength concrete beams reinforced with fiber-reinforced polymer bars," *ACI Structural Journal*, vol. 103, no. 3, pp. 383–389, 2006.

[43] S. P. Gross, J. R. Yost, D. W. Dinehart, E. Svensen, and N. Liu, "Shear strength of normal and high strength concrete beams reinforced with GFRP bars," in *4th International Conference on Advanced Composite Materials in Bridges and Structures, ACMBS*, 2004.

[44] Y. Mizukawa, Y. Sato, T. Ueda, and Y. Kakuta, "A study on shear fatigue behavior of concrete beams with FRP rods," in *International symposium; 3rd, Non-metallic (FRP) reinforcement for concrete structures*, Sapporo, Japan, 1997.

[45] H. Nakamura and T. Higai, "Evaluation of shear strength of concrete beams reinforced with FRP," *Proceedings of the Japan Society of Civil Engineers*, vol. 26, pp. 111–123, 1995.

[46] A. G. Razaqpur, B. O. Isgor, S. Greenaway, and A. Selley, "Concrete contribution to the shear resistance of fiber reinforced polymer reinforced concrete members," *Journal of Composites for Construction*, vol. 8, no. 5, pp. 452–460, 2004.

[47] R. N. Swamy and M. Aburawi, "Structural implications of using GFRP bars as concrete reinforcement," in *Proceedings of 3rd International Symposium, FRPRCS*, Tokyo, Japan, 1997.

[48] M. Tariq and J. Newhook, "Shear testing of FRP reinforced concrete without transverse reinforcement," in *Proceedings of the Annual Conference of the Canadian Society for Civil Engineering, CSCE*, Moncton, New Brunswick, Canada, 2003.

[49] A. K. Tureyen and R. J. Frosch, "Shear tests of FRP-reinforced concrete beams without stirrups," *ACI Structural Journal*, vol. 99, no. 4, pp. 427–434, 2002.

[50] J. R. Yost, S. P. Gross, and D. W. Dinehart, "Shear strength of normal strength concrete beams reinforced with deformed GFRP bars," *Journal of Composites for Construction*, vol. 5, no. 4, pp. 268–275, 2001.

[51] W. J. Zhao, K. Maruyama, and H. Suzuky, "Shear behavior of concrete beams reinforced by FRP rods as longitudinal and shear reinforcement," in *2nd International symposium, Nonmetallic (FRP) reinforcement for concrete structures*, Ghent, Belgium, 1995.

[52] S. Tottori and H. Wakui, "Shear capacity of RC and PC beams using FRP reinforcement," *ACI Special Publication*, vol. 138, pp. 615–632, 1993.

[53] F. Akgul, *Lifetime System Reliability Prediction for Multiple Structure Types in a Bridge Network*, University of Colorado at Boulder, Ann Arbor, MI, USA, 2002.

[54] M. P. Enright and D. M. Frangopol, "Probabilistic analysis of resistance degradation of reinforced concrete bridge beams under corrosion," *Engineering Structures*, vol. 20, no. 11, pp. 960–971, 1998.

[55] A. E. Naaman and A. Siriaksorn, "Reliability analysis of partially prestressed beams," in *Proceedings of the Sino-American Symposium on Bridge and Structural Engineering*, Beijing, China, 1983.

[56] A. Nowak, E. Szeliga, and M. Szerszen, *Reliability-based calibration for structural concrete, phase 3. Serial no. 2849*, Portland Cement Association Research and Development, 2008.

[57] M. P. Collins, E. C. Bentz, E. G. Sherwood, and L. Xie, "An adequate theory for the shear strength of reinforced concrete structures," *Magazine of Concrete Research*, vol. 60, no. 9, pp. 635–650, 2008.

[58] P. S. Marsh and D. M. Frangopol, "Reinforced concrete bridge deck reliability model incorporating temporal and spatial variations of probabilistic corrosion rate sensor data," *Reliability Engineering & System Safety*, vol. 93, no. 3, pp. 394–409, 2008.

[59] SHRP 2, *Bridges for Service Life Beyond 100 Years: Service Limit State Design, in Strategic Highway Research Program (SHRP) Report S2-R19B-RW-1*, Transportation Research Board, 2015.

[60] M. Robert and B. Benmokrane, "Behavior of GFRP reinforcing bars subjected to extreme temperatures," *Journal of Composites for Construction*, vol. 14, no. 4, pp. 353–360, 2010.

[61] A. Nowak and K. Collins, *Reliability of Structures*, Mcgraw-Hill Companies, Inc, 2000.

[62] AASHTO, *Guide Manual for Condition Evaluation and Load and Resistance Factor Rating (LRFR) of Highway Bridges*, American Association of Highway and Transportation Officials, Washington, DC, 2003.